Elastic Scattering of Oxygen Ions by Carbon, Magnesium, and Aluminum

J. A. KUEHNER, E. ALMQVIST, AND D. A. BROMLEY*
Atomic Energy of Canada Limited, Chalk River, Ontario, Canada
(Received 28 March 1963)

Elastic scattering measurements have been carried out on the O+C, O+Mg, and O+Al systems using beams of O^{16} ions of precisely defined energy from the Chalk River tandem accelerator. Measurements have been made for energies near and above the Coulomb barrier appropriate to each system. Evidence for sharp ($\Gamma\sim300$ keV) resonance structure is contained in a yield curve for O+C at a center-of-mass angle of 90°. This evidence is used to estimate $\Gamma_{\text{elastic}}/\Gamma$ for the resonant states to be ~7–10%. It is suggested that the resonant states involved may be similar to the "quasimolecular" states postulated to play an important role in the case of C+C scattering, although their appearance only at energies well above the Coulomb barrier, in contrast to the situation in C+C scattering, may allow a more conventional explanation. In the case of angular distributions for O+C, but not for O+Mg and O+Al, well-developed diffraction structure is observed. It is found that the simple sharp-cutoff models do not account quantitatively for the data although they do give the same qualitative features.

INTRODUCTION

MEASUREMENTS of heavy-ion elastic scattering have been carried out using N^{14} beams from the 63-in. Oak Ridge cyclotron[1] and beams of C^{12}, N^{14}, O^{16}, F^{19}, and Ne^{20} from the heavy-ion linear accelerators at Berkeley[2] and Yale.[3] In general, these experiments have consisted of the measurement of angular distributions at fixed energy. Since energy changes were effected by the use of absorbing material the energy resolution was limited by the energy spread of the resulting beam.

The advent of the tandem accelerator a few years ago made possible high resolution studies of heavy-ion elastic scattering in the energy range near the top of the Coulomb barrier for light targets. These high resolution measurements[4] have revealed unexpected sharp resonance structure for $C^{12}+C^{12}$ scattering which is not present in $O^{16}+O^{16}$ scattering. This paper reports evidence for similar resonance structure in $O^{16}+C^{12}$ scattering. In addition, measurements of angular distributions in $O^{16}+C^{12}$ scattering have been carried out at a number of energies; these angular distributions reveal a well-developed diffraction structure. Measurements of O^{16} scattered from Mg and Al are also reported. Further measurements of elastic scattering involving beams of C^{12}, N^{14} and O^{16} and an optical-model analysis of some of these data are presented elsewhere.[5,6]

EXPERIMENTAL TECHNIQUES

The scattering chamber used for these measurements has been described previously.[4] The detectors were Ortec Au-Si surface barrier counters or diffused *pn* junction detectors supplied by the counter development group at Chalk River. The counters were connected to Ortec Model 101 charge amplifiers followed by conventional voltage amplifiers and 100-channel pulse-height analyzers. The geometric arrangement was as follows: beam spot diameter on target = 1.8 mm, counter diameter = 1.5 mm, and target spot to counter separation = 133 mm. From these dimensions were computed the following: (i) the maximum spread in counter acceptance angle in the laboratory system was ±0.7° about the chosen angle setting; (ii) the detector solid angle was 1.0×10^{-4} sr.

Self-supporting targets of carbon (~10 μg/cm²), magnesium (~100 μg/cm²), and aluminum (~50 μg/cm²), all of natural isotopic composition, were prepared by evaporation. The technique in the case of carbon is described in Ref. 4. O^{16} ion beam energies in the range from 12 to 36 MeV in the laboratory system were obtained from the tandem accelerator with an energy resolution ~5 parts in 10^4; the absolute energy calibration is known to ±50 keV in the laboratory system. The energy loss of the beam in traversing the target material is estimated at ~33 keV in the center-of-mass system in the case of carbon, and ~380 and ~190 keV in the cases of magnesium and aluminum, respectively.

Angular distributions for O^{16} plus carbon elastic scattering have been measured at a number of energies in the range 8.0–13.67 MeV in the center-of-mass system and for O^{16} plus magneisum and aluminum at 19.1 and 20.0 MeV in the center-of-mass system, respectively. Measurements were also made of the O^{16} plus carbon elastic scattering yield as a function of the bombarding energy at center-of-mass angles of 59°, 72°, and 90°.

In the early measurements, including the angular distributions for O^{16} plus carbon at 11.57 and 13.67 MeV and for O^{16} plus magnesium and aluminum, a monitor counter fixed at 30° to the beam continuously monitored

---

* Present address: Yale University, New Haven, Connecticut.
[1] H. L. Reynolds and A. Zucker, Phys. Rev. **102**, 1378 (1956); M. L. Halbert and A. Zucker, *ibid.* **115**, 1635 (1959); M. L. Halbert, C. E. Hunting, and A. Zucker, *ibid.* **117**, 1545 (1960); M. L. Halbert and A. Zucker, Nucl. Phys. **16**, 158 (1960).
[2] E. Goldberg and H. L. Reynolds, Phys. Rev. **112**, 1981 (1958); M. L. Reynolds, E. Goldberg, and D. D. Kerlee, *ibid.* **119**, 2009 (1960); D. D. Kerlee, H. L. Reynolds, and E. Goldberg, *ibid.* **127**, 1224 (1962).
[3] J. A. McIntyre, S. D. Baker and T. L. Watts, Phys. Rev. **116**, 1212 (1959); E. Newman, P. G. Roll, and F. E. Steigert, *ibid.* **122**, 1842 (1961); P. G. Roll, E. Newman, and F. E. Steigert, Nucl. Phys. **29**, 544 (1962); J. A. McIntyre, S. D. Baker, and K. H. Wang, Phys. Rev. **125**, 584 (1962); J. E. Kelley, F. E. Steigert, and W. W. Watson, *ibid.* **126**, 2100 (1962); K. H. Wang, S. D. Baker, and J. A. McIntyre, *ibid.* **127**, 187 (1962).
[4] D. A. Bromley, J. A. Kuehner, and E. Almqvist, Phys. Rev. Letters **4**, 365 (1960); Phys. Rev. **123**, 878 (1961).
[5] J. A. Kuehner and E. Almqvist (to be published).
[6] J. A. Kuehner and E. Almqvist (to be published).

the scattering, thus, providing normalization of both the beam intensity and the number of target atoms. It became apparent during the course of the measurements that a more accurate absolute normalization of the cross-section scale could be obtained by the use of a target on which was a thin layer of gold. Thus, for the measurements of excitation curves and for the O^{16} plus carbon angular distributions measured at 8, 9, and 10 MeV the procedure described below was used. A subsequent check of the angular distribution for O^{16} plus carbon at 13.67 MeV using the technique described below confirmed the accuracy of the early measurements.

For sufficiently low energies pure Coulomb scattering ($d\sigma \propto E^{-2}$) is obtained. This fact was used to calibrate the equipment to permit accurate measurement of the ratio of the cross section to the Coulomb cross section. In practice the quantity measured was the ratio of the scattering yield from carbon to that observed simultaneously from a thin layer ($\sim 1\ \mu g/cm^2$) of gold deposited on the carbon target. When the scattering from both carbon and gold obey the Coulomb law, as they will at sufficiently low energies, this ratio is constant and independent of energy; this constant value is normalized to unity. With this normalization the measured ratio at higher energies is directly the ratio $d\sigma/d\sigma_{\text{Coulomb}}$ for scattering from carbon (the scattering from gold is assumed to be pure Coulomb scattering at all energies used).

The method just described for determining the ratio $d\sigma/d\sigma_{\text{Coulomb}}$ has the great advantage that no measure is required of either the beam intensity or of the number of target atoms per unit area. However, as outlined, it assumes that the ratio of the number of carbon atoms to gold atoms in the target remains constant throughout the measurements. This is, of course, not true chiefly because of carbon build up and to a slight extent because of gold sputtering away under bombardment. The slow rate of change of the target composition was monitored

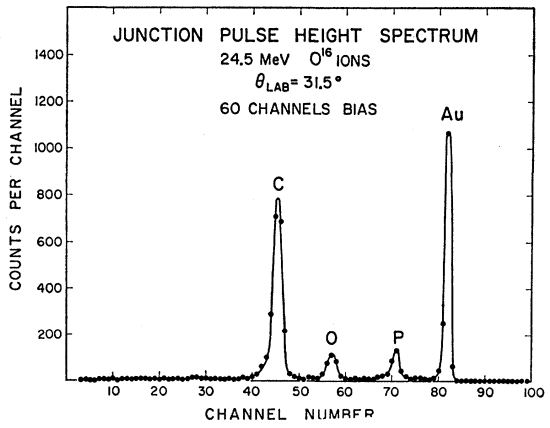

FIG. 1. Pulse-height spectrum measured for 24.5-MeV O^{16} ions on an $\sim 10\ \mu g/cm^2$ carbon target with $\sim 1\ \mu g/cm^2$ gold. Peaks labeled C, O, P, and Au result from O^{16} ions scattered from carbon, oxygen, phosphorus, and gold, respectively.

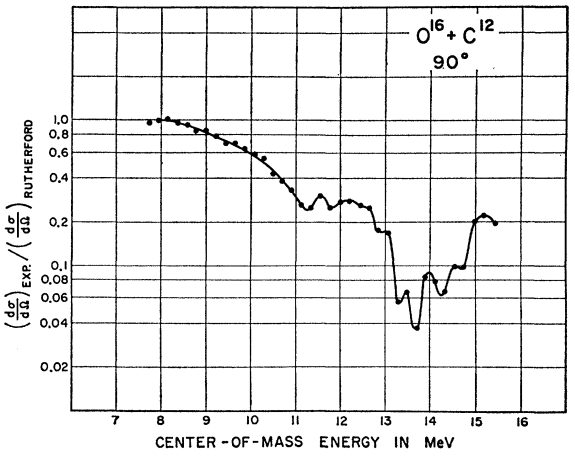

FIG. 2. Excitation curve for $O^{16}+C^{12}$ elastic scattering measured at a center-of-mass angle of 90°.

by periodically repeating measurements made earlier. From the repeated data it is estimated that corrections for changes in target composition could be made to an accuracy of $\pm 1\%$. In addition, for the angular distribution measurements the fixed counter continuously monitored the scattering from the carbon and gold on the target, thus, making the results independent of target composition changes.

RESULTS

Figure 1 shows a typical spectrum measured for 24.5-MeV O^{16} ions on an $\sim 10\ \mu g/cm^2$ carbon target with $\sim 1\ \mu g/cm^2$ gold. The scattered O^{16} ions from the main target components are labeled C and Au. Additional peaks labeled O and P result from O^{16} ions scattered from oxygen and phosphorus contaminants in the target.

The peaks in the pulse-height spectra corresponding to particles scattered from carbon and from gold were completely resolved from much weaker groups resulting from scattering by the contaminant elements in the targets except at angles forward of $\sim 22°$ in the laboratory system ($\sim 52°$ c.m. for $O^{16}+C^{12}$). At the most forward angles, therefore, the assignment of errors is more difficult and an additional check of some of the data was made using the recoil coincidence method[7] to discriminate better against contaminants.

At angles greater than $\sim 42°$ in the laboratory system (112° c.m. for $O^{16}+C^{12}$) the energy and, hence, pulse height as well as intensity of the scattered particle group becomes small and an appreciable uncertainty arises because of a background continuum of pulses. Thus, the values of $d\sigma/d\sigma_{\text{Coulomb}}$ for θ_{lab} greater than 42° represent upper limits to the cross sections.

Figure 2 shows the elastic scattering excitation curve for $O^{16}+$carbon measured at a center-of-mass angle of 90°. Subsequent measurements using a thinner target show that the minimum at 13.67 MeV is somewhat

[7] M. L. Halbert and A. Zucker, Phys. Rev. **115**, 1635 (1959).

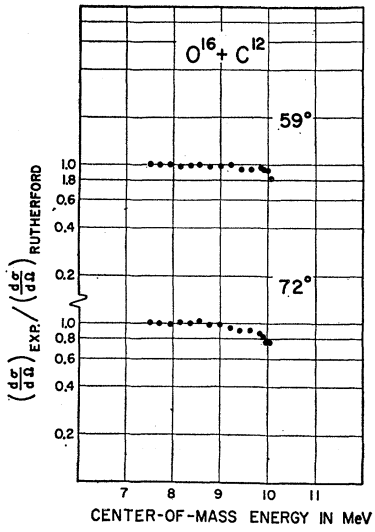

FIG. 3. Excitation curves for $O^{16}+C^{12}$ elastic scattering measured at center-of-mass angles of 59° (top) and 72° (bottom).

deeper than indicated in Fig. 2 and corresponds to the value found at 90° in the angular distribution at this energy (Fig. 5), for which a thin target was used. Figure 3 shows similar curves measured over a smaller energy range for center-of-mass angles of 59° and 72°. Figures 4 and 5 show elastic scattering angular distributions for O^{16}+carbon measured at center-of-mass energies of 8.0, 9.0, 10.0, 11.57, and 13.67 MeV, respectively. Figure 6 shows elastic scattering angular distributions for O^{16}+magnesium and O^{16}+aluminum measured at center-of-mass energies of 19.1 and 20.0 MeV, respectively. The curves included in Figs. 2–6 are simply drawn to connect the experimental points.

The standard deviations reflecting counting statistics for those data measured using the ratio to scattering from Au are ~2–4% over most of the range of angles studied; an exception are those data at large angles where the standard deviations resulting from counting statistics rise to ~6–8%. Additional instrumental uncertainties are estimated as follows: (i) Angle setting is accurate to ±0.1° relative values and ±0.3° absolute values in the laboratory system; (ii) the center of the beam spot on the target is located within ±0.5 mm of the chamber axis, i.e. the target spot to detector distance is kept constant to within ±0.4%. A check on the magnitude of the instrumental errors is given by the observed scattering from gold, which closely follows the expected $\csc^4(\theta/2)$ angular dependence.

DISCUSSION

A. Diffraction Effects

Inspection of the angular distributions for $O^{16}+C^{12}$ in Figs. 4 and 5 suggests a diffraction effect resulting in an oscillatory behavior of the differential cross section. Accordingly, some attempts were made to account for these results using the sharp-cutoff model,[8] which has had success in accounting for alpha-particle and heavy-ion elastic scattering at higher energies and which predicts an oscillatory angular distribution. In this model it is assumed that the nuclear interaction occurs only within a certain well-defined radius; all partial waves corresponding to classical trajectories which lie within this radius are assumed to be completely absorbed while those remaining are assumed to be unaffected by the nuclear interaction apart from the Coulomb force. The "cutoff" partial wave is obtained by equating the kinetic energy to the sum of the Coulomb energy and the angular momentum energy at the interaction radius. Thus, the "cutoff" angular momentum, l_c, is given by

$$E=\frac{Z_1Z_2e^2}{R}+\frac{l_c(l_c+1)\hbar^2}{2MR^2}. \quad (1)$$

The differential cross section is then given by

$$\frac{d\sigma}{d\Omega}=\left(\frac{Z_1Z_2e^2}{4E}\right)^2\left|\csc^2(\tfrac{1}{2}\theta)\exp\{-i\eta\ln\sin^2(\tfrac{1}{2}\theta)\}\right.$$
$$\left.-\frac{i}{\eta}\sum(2l+1)P_l(\cos\theta)\exp(2i\delta_l)(1-A_l)\right|^2, \quad (2)$$

where $A_l=0$ for $0\leq l\leq l_c$, $A_l=1$ for $l>l_c$. In (2) δ_l is the Coulomb phase shift given by $\delta_l=\sum_{k=1}^{l}\tan^{-1}(\eta/k)$, $l>0$, and $\delta_0=0$. η is the Sommerfeld parameter given by $\eta=Z_1Z_2e^2/\hbar v$.

Obviously l_c depends on the interaction radius, R, which is assumed. There is, thus, one adjustable parameter in this model.

Figure 7 contains, at the top and at the bottom, sharp-cutoff model curves (solid curves) together with the data for 11.57-MeV $O^{16}+C^{12}$ scattering. The values of l_c used correspond to radius constants, r_0, as labeled in the figure; r_0 is related to R through $R=r_0(A_1^{1/3}+A_2^{1/3})$. Obviously, neither of these curves agrees with the

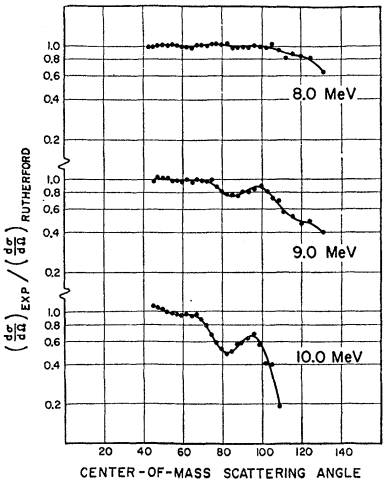

FIG. 4. $O^{16}+C^{12}$ elastic-scattering angular distributions measured at center-of-mass energies of 8.0 MeV (top), 9.0 MeV (middle), and 10.0 MeV (bottom).

[8] J. S. Blair, Phys. Rev. **95**, 1218 (1954); **108**, 827 (1957); D. D. Kerlee, J. S. Blair, and G. W. Farwell, *ibid.* **107**, 1343 (1957).

measurements, although they do have the right sort of qualitative features. At first sight, it appears that better agreement could be obtained through the use of an interpolation procedure, thus allowing the minima and maxima to be more closely fitted. In doing so, however, one must not lose sight of the fact that the sharp-cutoff or "black nucleus" model is only approximate, and, as Austern[9] has pointed out, does not agree at all well with the results of a simple complex well optical model. Nevertheless, it may be instructive to carry this simple approach one step further by the use of a model allowing a continuous or "smoothed" cutoff in l. One such method,[10] which also allows the cutoff to be made less sharp, assumes a continuous cutoff in l with A_l taking the form

$$A_l=\left[1+\exp\left(\frac{l_c-l}{\Delta l}\right)\right]^{-1}. \quad (3)$$

This model contains one more prameter, Δl, which is related to a surface thickness, ΔR, through

$$\Delta l=2\rho(\rho-\eta)(\Delta R/R)(2l_c+1)^{-1}, \quad (4)$$

where ρ is given by $\rho=mvR/\hbar$.

This "smoothed"-cutoff model is continuous in the cutoff of l and allows interpolation between the curves in Fig. 7. Unfortunately, even with Δl kept small this interpolation procedure necessarily damps the size of the oscillations. This is shown by the middle curve in Fig. 7 which correspond to $l_c=7$ and $\Delta l\ll 1$. Thus, the sharp-cutoff curves at the top and bottom of Fig. 7 interpolate from one to the other by going through the curve in the middle of Fig. 7. It appears from this that the positions and sizes of the oscillations cannot be adjusted sufficiently independently with this model to fit these data.

Of course, it may turn out that at a different energy better success can be obtained with this model. This is illustrated in Fig. 8 where the upper curve, A, is able to give the positions of the extrema for the 13.67-MeV $O^{16}+C^{12}$ data reasonably well. However, curve A fails badly in giving the magnitude of the cross section. Better agreement in magnitude can be obtained by using a larger radius constant as in curve B of Fig. 8. However, the positions of the extrema are now not given correctly. Within the framework of this two-parameter model agreement with the magnitude of the cross section can be obtained only at the expense of poor agreement with the positions of the extrema.

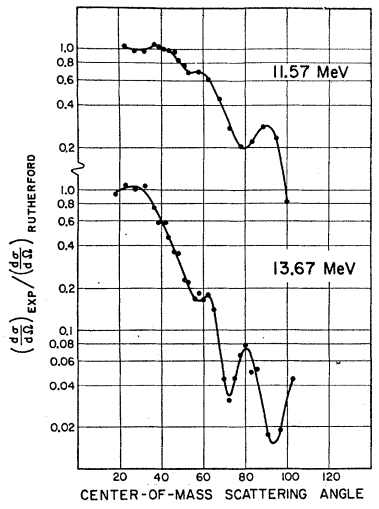

FIG. 5. $O^{16}+C^{12}$ elastic scattering angular distributions measured at center-of-mass energies of 11.57 MeV (top) and 13.67 MeV (bottom).

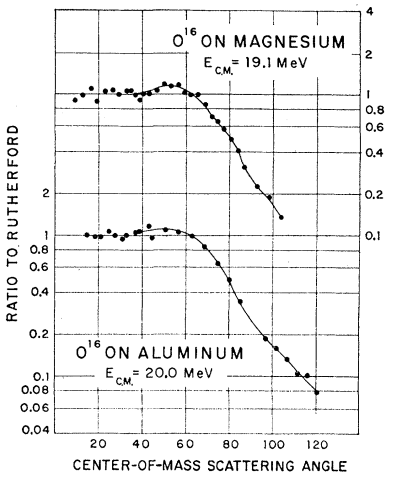

FIG. 6. Elastic scattering angular distributions for O^{16}+magnesium at $E_{c.m.}=19.1$ MeV (top) and O^{16}+aluminum at $E_{c.m.}=20.0$ MeV (bottom).

In both the 11.57- and the 13.67-MeV cases the radius constant giving best agreement with the positions of the extrema ($r_0\sim 1.5$ F) is considerably smaller than that giving best agreement with the absolute magnitudes of the cross sections ($r_0\sim 1.7$–1.9 F). Both of these radius constants are considerably larger than that obtained in a typical optical-model fit[6,11] ($r_0\sim 1.2$ F). Blair[12] has suggested that the reason for a larger radius in the sharp-cutoff model than in the corresponding optical model is that in the sharp-cutoff model the radius corresponds to the position of the maximum of the potential barrier. This radius is considerably larger than the "one-half" value point of the corresponding nuclear potential. This appears to account qualitatively for the large radii obtained for the sharp-cutoff model in Figs. 7 and 8. The larger radius constant obtained in the sharp-cutoff model to give the absolute value of the cross section as compared to that required to give the right sort of diffraction structure probably reflects the importance of quantum-mechanical penetration of high order partial waves ($l>l_c$) in these low energy cases.

The fact that the experimental magnitudes of the diffraction oscillations are nearly as large as those given by the sharp-cutoff model suggests that the diffraction mechanism does play a major role in this case.

The relatively poor quantitative agreement between these simple models and the measurements together

[9] N. Austern, Ann. Phys. (N. Y.) **15**, 299 (1961).
[10] J. A. McIntyre, K. H. Wang, and L. C. Becker, Phys. Rev. **117**, 1337 (1960).
[11] C. E. Porter, Phys. Rev. **112**, 1722 (1958).
[12] J. S. Blair, Phys. Rev. **108**, 827 (1957).

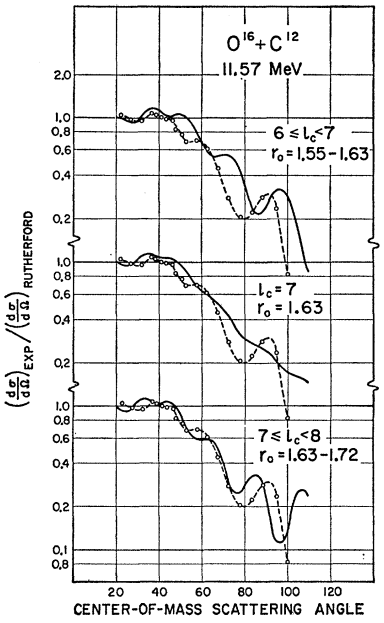

FIG. 7. Sharp-cutoff model curves (solid lines) are compared with the $O^{16}+C^{12}$ elastic scattering angular distributions for 11.57 MeV. The curves at the top and bottom are obtained using the simple sharp-cutoff model. The curve in the middle uses a "rounded"-cutoff model to allow interpolation between the curves at the top and at the bottom. The reader is referred to the text for definitions of the model parameters.

with reasonably good qualitative agreement suggest that the addition of more parameters, for example, a complex nuclear phase shift, might produce better agreement. It was felt, however, that rather than search for fits with such a semiempirical model one might gain more insight into the physical processes by instead using a complex optical potential model. A search for fits to these data as well as to other data using such an optical model are presented elsewhere.[6]

In contrast to the O^{16} plus carbon case the angular distributions for O^{16} plus magnesium and O^{16} plus aluminum, contained in Fig. 6, show little or no diffraction structure. This agrees with the empirical trend observed by McIntyre *et al.*[13] that the size of the diffraction structure depends on η and appears strongly only for those cases for which $\eta \lesssim 5$. Table I gives values of $E_{\text{c.m.}}$ and η for the scattering systems reported in this paper. The $O^{16}+C^{12}$ system appears to be an exception to the rule, however, since it exhibits very marked diffraction although $\eta \gtrsim 5$. As discussed elsewhere,[6] this may result from an exceptionally large interpenetration of the C^{12} and O^{16} ions.

B. Resonant Effects

As indicated in Fig. 2, $O^{16}+C^{12}$ exhibits resonant effects similar to those observed in $C^{12}+C^{12}$ scattering[4] which have been interpreted as resulting from the formation of "quasimolecular" states which tend to decay into the elastic channel with rather large probability. It appears that in the case of $O^{16}+C^{12}$, also, this mechaism is of importance.

It is suggested by the optical model analysis[6] that the broad structure in the yield curve, e.g. the over-all rise in $d\sigma/d\sigma_c$ for energies above 13.5 MeV, is the result of the diffraction nature of the process. It is the narrow structure, $\Gamma \sim 300$ keV, which may be due to "quasimolecular" states.

As in the case of $C^{12}+C^{12}$ scattering it is possible to obtain an estimate of the widths for compound elastic scattering from the magnitudes of the resonance effects displayed in the differential excitation function. It is most likely that overlapping resonances are involved; however, by assuming a single resonace to be responsible mainly for the most rapidly varying resonance fluctuations an estimate of the elastic width can be made. It is likely that this will lead to a lower limit for the widths since, in general, the effects of many overlapping levels will tend to cancel each other out.

The effect on the elastic scattering of a single resonance can be obtained from the expression for the scattering cross section

$$\frac{d\sigma}{d\Omega}=\left(\frac{Z_1Z_2e^2}{4E}\right)^2\Bigg|\csc^2(\tfrac{1}{2}\theta)\exp\{-i\eta\ln\sin^2(\tfrac{1}{2}\theta)\}$$

$$-\frac{i}{\eta}\sum(2l+1)P_l(\cos\theta)\exp(2i\delta_l)[1-\exp(2iu_l)]$$

$$-\frac{i}{\eta}(2l'+1)P_{l'}(\cos\theta)\exp(2i\delta_{l'})$$

$$\times\exp(2iu_{l'})\frac{i\Gamma_{\text{el}}}{(E-E_0)+\frac{1}{2}i\Gamma}\Bigg|^2, \quad (5)$$

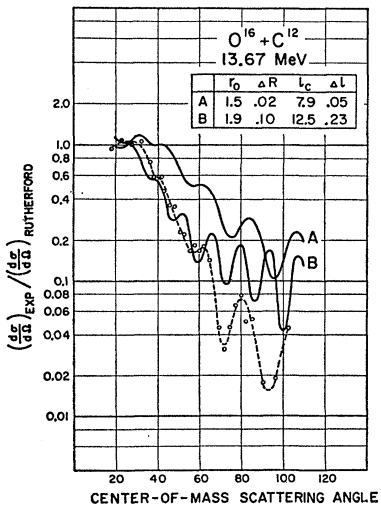

FIG. 8. Sharp-cutoff model curves (solid lines) using a transition region for the angular momentum cutoff are compared with the $O^{16}+C^{12}$ elastic scattering angular distributions for 13.67 MeV. The model parameters are included in the inset table.

[13] J. A. McIntyre, S. D. Baker, and T. L. Watts, Phys. Rev. **116**, 1212 (1959).

TABLE I. Values of the center-of-mass energy, $E_{c.m.}$, and the Sommerfeld parameter, $=Z_1Z_2e^2/\hbar v$, are listed for the scattering systems reported in this paper.

	$E_{c.m.}$ (MeV)	η
$O^{16}+C^{12}$	8.0–13.67	7.0–5.4
$O^{16}+Mg^{24}$	19.1	10.7
$O^{16}+Al^{27}$	20.0	11.6

where δ_l and u_l are the Coulomb and nuclear phase shifts, respectively, Γ_{el} is the elastic width and l' is the resonant angular momentum. In Fig. 2 fluctuations of $\sim 50\%$ are observed in a region where $d\sigma/d\sigma_{\text{Coulomb}}$ is ~ 0.1. Thus, we can write

$$\left(\frac{d\sigma}{d\Omega}\right)\Big/\left(\frac{d\sigma}{d\Omega}\right)_{\text{Coulomb}} = \frac{|A+\sum B_l[1-\exp(2iu_l)]|^2}{|A|^2} \sim 0.1, \quad (6)$$

where A and B_l are defined by inspection from (5). At $\theta=90°$ $|A|^2=4$ so that

$$|A+\sum B_l[1-\exp(2iu_l)]| \sim (4\times 0.1)^{1/2}. \quad (7)$$

In order to produce fluctuations of 50% we must have

$$(|B_{l'}|\Gamma_{el})/\Gamma \sim \frac{(1.5)^{1/2}-1}{(1.5)^{1/2}+1}\times(4\times 0.1)^{1/2},$$

whence

$$\Gamma_{el}/\Gamma \sim 0.064/|B_{l'}| \simeq \frac{0.064\eta}{(2l'+1)|P_{l'}(\cos\theta)|} \simeq \frac{0.34}{(2l'+1)|P_{l'}(\cos\theta)|}.$$

This leads to values of Γ_{el}/Γ ranging from 7% to 10% for resonant angular momenta in the range 4 to 10.

This estimate of Γ_{el}/Γ is $\sim\frac{1}{2}$ as large as in the case of C^{12} plus C^{12} scattering. It, thus, appears that in the case of $O^{16}+C^{12}$, as well as in $C^{12}+C^{12}$, unexpectedly large resonant elastic widths are implied by the fluctuations observed in the differential cross sections. This is in marked contrast to the situation observed in other systems such as[4] in $O^{16}+O^{16}$ or in[5] $O^{16}+Be^9$. The large resonant elastic widths observed suggest a connection between the states involved and the "quasimolecular" states observed at energies nearer the barrier in $C^{12}+C^{12}$ reactions.[14] A discussion of several explanations[15] put forward to describe these states is contained in Ref. 14.

It should be pointed out that in contrast to the $C^{12}+C^{12}$ scattering, where strong resonant effects were observed at energies very near the barrier as well as at higher energies, the $O^{16}+C^{12}$ scattering exhibits strong resonant effects only at higher energies. At these higher energies it is possible that the mechanism responsible for the long-lived states is different than at the lower energies. This may result from a tendency at higher energies for the larger values of angular momentum involved to be sufficient to cause large permanent deformations of the nucleus with much of the energy of excitation tied up in deformation energy. Under these conditions less energy is available to boil off nucleons. On the other hand, decay into large fragments would tend to be enhanced. An additional inhibition of nucleon decay channels will result from their reduced ability to carry away the large values of angular momentum required. These effects may be sufficient to account for the large relative elastic widths and long lifetimes observed.

Although the resonant effects observed for $O^{16}+C^{12}$ and those observed for $C^{12}+C^{12}$ at energies well above the barrier may allow a different explanation than is required to explain those observed for $C^{12}+C^{12}$ near the barrier it is not clear why similar effects should not be observed in other systems.

CONCLUSIONS

Measurements of the elastic scattering of O^{16} on C, Mg and Al have been made for energies near and just above the Coulomb barrier. In the case of $O^{16}+C^{12}$, well-developed diffraction structure is observed. It is found that the simple sharp-cutoff models do not account quantitatively for the data although they do give the same qualitative features.

Evidence for sharp resonance structure is contained in the $O^{16}+C^{12}$ yield curve. This evidence is used to estimate $\Gamma_{\text{elastic}}/\Gamma$ for $O^{16}+C^{12}$ to be ~ 7–10%. It is suggested that the resonant states involved may be similar to the "quasimolecular" states postulated to play an important role in the case of $C^{12}+C^{12}$ scattering, although their appearance only at energies well above the Coulomb barrier, in contrast to the situation in $C^{12}+C^{12}$ scattering, may allow a more conventional explanation involving angular momentum arguments.

[14] E. Almqvist, D. A. Bromley, and J. A. Kuehner, Phys. Rev. Letters **4**, 515 (1960); E. Almqvist, D. A. Bromley, J. A. Kuehner, and B. Whalen, Phys. Rev. **130**, 1140 (1963).

[15] E. W. Vogt and H. McManus, Phys. Rev. Letters **4**, 518 (1960); R. H. Davis, *ibid.* **4**, 521 (1960); D. R. Inglis (private communication); K. Wildermuth and R. L. Carovillano, Nucl. Phys. **28**, 636 (1961); A. S. Kompaneets, Zh. Eksperim. i Teor. Fiz. **39**, 1713 (1960) [translation: Soviet Phys.—JETP **12**, 1196 (1961)].